International Journal of Theoretical Physics, Vol. 38, No. 1, 1999

What Is the State of a Hydrogen Atom Leaving a Stern–Gerlach Interferometer?

K. Brodsky,[1] F. Perales,[1] J. B. Lawson-Daku,[1] R. Mathevet,[1] J. Baudon,[1,2] and J. Robert[1,2,3]

Received August 7, 1998

We discuss experimental results on Stern–Gerlach interferometry with atoms. After a theoretical approach suited for fast atoms, we discuss elementary experiments on the preservation of atomic coherence. Then we examine the action of the interferometer as producing atoms with new properties, beaded atoms, and their radiative properties.

1. HISTORY AND MOTIVATIONS

1.1. Brief Introduction

Atom interferometry became popular in the 1990s, about 20 years after Sokolov's first experiment (Sokolov, 1973), mainly because most techniques of molecular beams and their control by microstructures or laser light became available at that time (Baudon, 1998). The Stern–Gerlach effect, on its own, had been quite disregarded, except by Bloom (1962), because of the remarkable efficiency of molecular beam resonance techniques (Rabi, 1937). With neutron beams, the first related experiment of magnetic interferometry was performed in 1938 (Frisch, 1938) and a revival of that work appeared and grew in the 1980s mainly by the neutron spin echo technique (Mezei, 1986). Two groups are currently using Stern–Gerlach interferometry (SGI) with atoms, one in Villetaneuse (Robert, 1991, 1992; Lawson, 1996; Mathevet, 1997) and more recently another one in Heidelberg (DeKieviet, 1995).

[1] Laboratoire de Physique des Lasers, UMR 7538 du CNRS, Université Paris Nord, 93430 Villetaneuse, France; e-mail: name@lpl.univ-paris13.fr.
[2] Fondation Louis de Broglie, 75006 Paris, France.
[3] To whom correspondence should be addressed.

0020-7748/99/0100-025 9$16.00/0

Basically Stern–Gerlach interferometry makes use of the spin components individually. Quantum interferometry is rooted in the superposition principle. This principle of superposition of states has to be clearly separated from the representation of one state by an expansion over a basis set, even if the formulas look the same. Consequently the definition of the quantization axis is of particular importance, especially when this axis is not fixed, imposing on the spin components dynamical or "active" transformations. Two limiting situations may arise: (i) the direction of the magnetic field (the actual one or the effective one) is slowly varying, which results in an adiabatic following of the spin components, each corresponding to one arm of the interferometer; (ii) the field direction rotates rapidly, which leads to a nonadiabatic evolution of the spin components (Majorana transition). Such zones are key elements of the interferometer since they transform one incoming Zeeman state, referred to some initial adiabatic quantization axis, into a coherent superposition of Zeeman states referred to a new final adiabatic quantization axis. This transformation can be readily described by the use of Wigner rotation matrices. It is worth noting that the resulting superposition of states is not a simple theoretical artefact insofar as the quantization axis cannot be arbitrarily chosen, but is governed by the dynamics.

In short, an SGI works as follows (see Fig. 1): a collimated beam of atoms is first spin polarized, then a first diabatic transition zone (Majorana zone) separates the spin components defined on the adiabatic quantization axis of the interferometer core, each spin component defining an arm of the

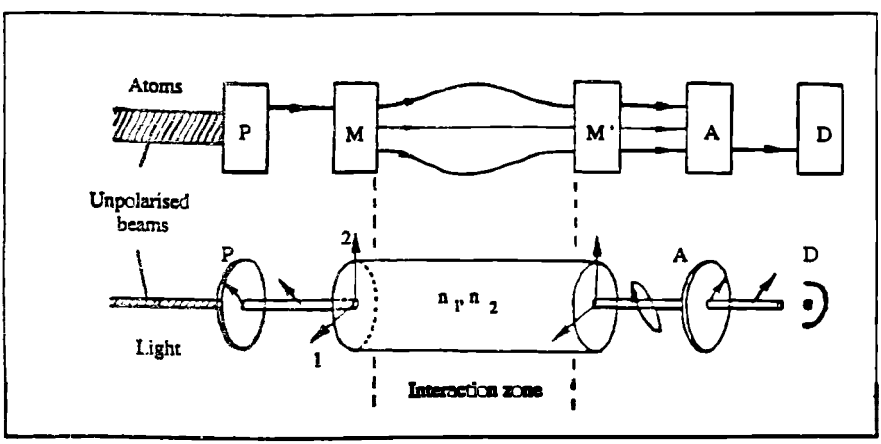

Fig. 1. Schematic diagram of the Stern–Gerlach atomic interferometer with its optical analogue. P is a polarizer, M and M′ are superposition regions at either extremity of the interaction region, A is an analyzer, and D is the detector. In the optical analogue the interaction zone consists of a birefringent medium of indices n_1 and n_2 corresponding to the polarization eigenvectors 1 and 2.

interferometer. Then, a second Majorana transition zone closes the interferometer with respect to the spin variable. The separated arm evolutions are converted for each spin component on the new quantization axis. A polarizer selects one of these, whose population reflects the whole history of the atom in the device. Then the signal on the detector exhibits fringes when one of the experiment's parameters is scanned.

What are the salient characteristics of an SGI? (i) It makes use of the spatial quantization of spin. It acts on real space spinors and fully degenerate structures. (ii) Most of the field configurations are quasistatic fields (without any propagation effects) and so can be considered as well-defined classical fields. (iii) Its main principle relies on the entanglement of variables (electronic, spin, and center-of-mass motion) and the projection onto the spin variable reveals the phase properties of the other variables. (iv) It can operate at any atomic velocity.

1.2. Motivations

The SGI's characteristics allow one to study atomic beam coherence properties. A theoretical approach to this problem is given in Section 2. The main point is the separation of the atomic beam properties from those related to the interferometer device itself. In other words, the difficult choice is that of the wave packet to be associated with the atom beam, whose parameters include necessarily the geometric boundary conditions of the experiment, and which precludes the representation of these atoms by infinite plane waves. This aspect of the wave packet properties will be illustrated in Section 3. The next step is to test whether these wave packet properties can be stored in the atomic beam. This will mean that under special circumstances it will be possible to exhibit unexpected properties. As an illustration in Section 4 we present a naive tentative experimental investigation of these properties through the study of the angular dependence of the spontaneous decay of atoms leaving the interferometer (beaded atoms).

2. THEORETICAL ANALYSIS OF SGI USING FAST ATOMS

2.1. Wave Function Computation

To solve the wave function computation problem when using fast hydrogen atoms, we have to face two simultaneous problems. (i) That of the spin evolution in a nonuniform magnetic field, correctly described thanks to Schwinger (1937). (ii) The scattering of atoms by a macroscopic size potential region, which is a typical problem in atom interferometry; this problem can be reduced in our experimental configuration (fast atoms, $E_{\mathrm{Kin}} = 0.5$ eV, and very small magnetic energy, about a few neV) to that of atomic scattering

in high-energy approximation (Glauber, 1959), which makes use of eikonal and slowly varying envelope approximations.

In the semiquantal Glauber method, the adiabatic basis set is chosen as a plane wave symmetry expansion. The phase shifts are computed along the rays corresponding to incoming plane waves. This simplifies the resolution of the spin evolution problem for each component, because the rays and the magnetic field they cross are defined *ab initio*. One has just to sum up all the terms accumulated by each plane wave in order to get the wavefront distortion, which, in that picture, will reflect (once converted in terms of outgoing plane waves) the motion of the atoms at the output of the device (Fig. 2).

The use of plane waves makes the quantum potential terms vanish. The phase shift in that case is directly given in terms of the classical Hamilton–Jacobi solutions. We briefly review this method.

To solve the Schrödinger equation

$$i\hbar\partial_t\psi = (T + V)\psi \tag{2.1}$$

with the de Broglie parametrization for ψ,

$$\psi(\mathbf{r}, t) = a(\mathbf{r}, t)\exp[i(S(\mathbf{r}, t))/\hbar] \tag{2.2}$$

(a and S are real functions), we get the system (M is the mass of the particle)

$$\begin{cases} \partial_t S + \dfrac{1}{2M}(\nabla S)^2 + V - \dfrac{\hbar^2}{2M}\dfrac{\Delta a}{a} = 0 \\ \partial_t a + \dfrac{a}{2M}\Delta S + \dfrac{1}{M}\nabla S \cdot \nabla a = 0 \end{cases} \tag{2.3}$$

If we restrict ourselves to a constant function a, then $\Delta S = 0$. We get modulated plane wave solutions, which are exact solutions at least for potentials of the form $V(\mathbf{r}, t) = \mathbf{g}(t) \cdot \mathbf{r} + \omega(t)$.

However, in scattering problems, a difficulty arises because of the $\mathbf{r}$ dependence of the potential energy term. As shown by Glauber, when V is small compared to the incoming kinetic energy, it is possible to neglect reflection terms due to the rapid variations of the potential, i.e., backscattering terms and coupling between the incoming plane waves. Distorted plane wave solutions are constructed from incoming plane wave solutions [take $V = 0$ and $a = \text{const}$ in (2.3)] modulated by a slowly varying envelope,

$$\psi(\mathbf{r}, t) = [a(\mathbf{r}, t)e^{i\varphi(\mathbf{k},t)/\hbar}]\psi_P(\mathbf{k}; \mathbf{r}, t) \tag{2.4}$$

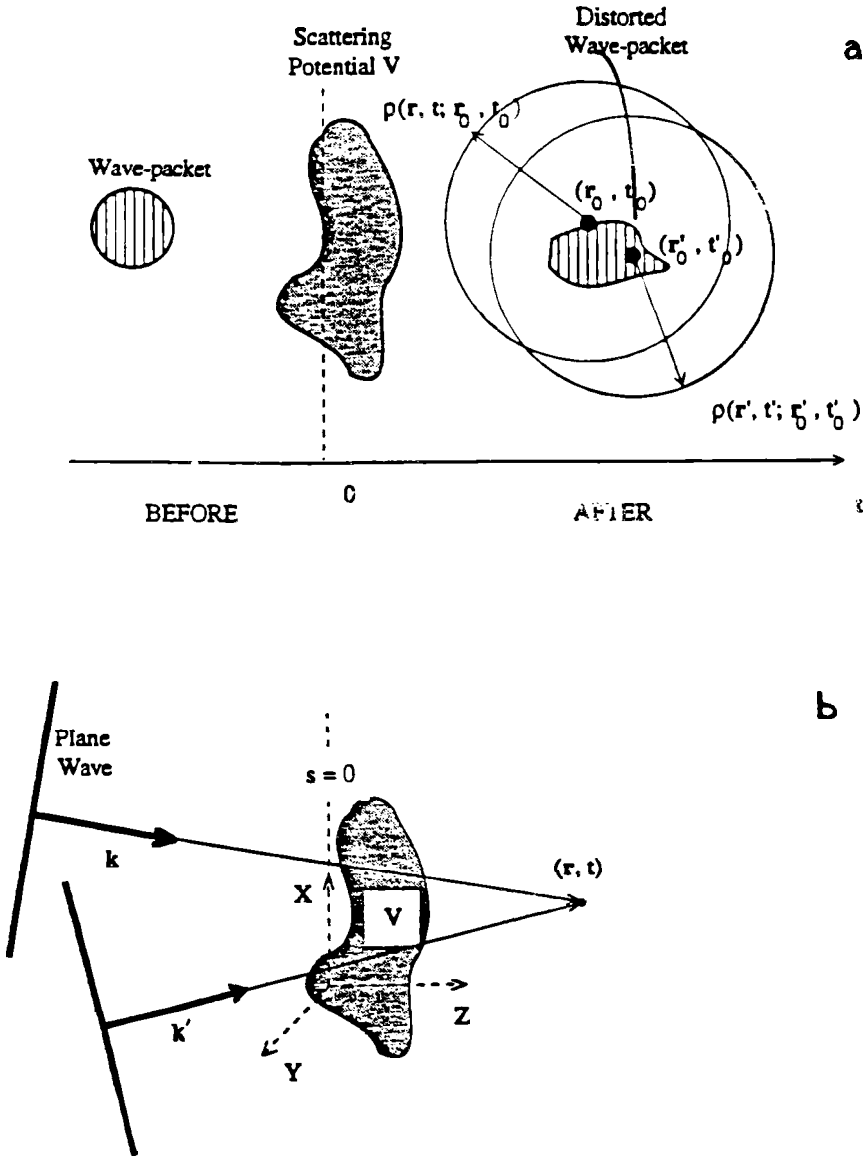

Fig. 2. (a) Schematic representation of the scattering process showing the incident wave packet, the scattering potential V, the outgoing distorted wave packet, and the detector domain $\rho(\mathbf{r}, t; \mathbf{r}_0, t_0)$ defined for each point $(\mathbf{r}_0, t_0)$. (b) Plane wave representation of the scattering process with two wave vectors $\mathbf{k}$, $\mathbf{k}'$ and their associated rays converging at the detector position.

where the real functions a and φ slowly vary at the wavelength scale. The incoming plane wave is

$$\psi_P(\mathbf{k}, \mathbf{r}, t) = e^{i\mathbf{k}\mathbf{r} - i\hbar(k^2/2M)t} \tag{2.5}$$

Neglecting higher order terms, a and φ obey the equations

$$\begin{cases} \partial_t \varphi + \dfrac{\hbar \mathbf{k}}{M} \cdot \nabla \varphi + V(\mathbf{r}, t) = 0 \\ \partial_t a + \dfrac{\hbar \mathbf{k}}{M} \cdot \nabla a = 0 \end{cases} \tag{2.6}$$

Then the perturbation in the wave moves with the group velocity $v\mathbf{u} = \hbar\mathbf{k}/M$, and ∇ and $\mathbf{r}$ can be reduced to

$$\begin{cases} \nabla = \mathbf{u}\partial_u + \nabla_\perp \\ \mathbf{r} = (\mathbf{r} \cdot \mathbf{u})\mathbf{u} + [\mathbf{r} - (\mathbf{r} \cdot \mathbf{u})\mathbf{u}] = u\mathbf{u} + \mathbf{r}_\perp \end{cases} \tag{2.7}$$

with $\mathbf{r}_\perp$ being the impact parameter. The amplitude is

$$a(\mathbf{r}, t) = a(\mathbf{r}_\perp, u - vt) \tag{2.8a}$$

Depending on the chosen integration variable, the phase shift can take two forms:

$$\begin{cases} \varphi(v, u - vt, t; \mathbf{r}_\perp) = \dfrac{1}{v} \displaystyle\int^u V(s)\, ds \\ \varphi(v, u, t - \dfrac{u}{v}; \mathbf{r}_\perp) = \displaystyle\int^t V(s)\, ds \end{cases} \tag{2.8b}$$

The second form shows that it is possible to make φ independent of v, giving rise to nondispersive effects (Nic Chormaic, 1994).

All the preceding expressions have to be modified in order to take into account the spin multiplicity. To get straightforward expressions, we assume that all the rays are subjected to the same Majorana transitions (same Wigner rotation matrix) and that their evolution in between follows the same quantizations axis. The validity of these points will be discussed in Section 3. With these restrictions the most general polarized incoming wave takes the form

$$\psi_\alpha^{\text{in}}(\mathbf{r}, t) = \int d^3k\, C_\alpha(\mathbf{k}) \psi_P(\mathbf{k}, \mathbf{r}, t) \tag{2.9}$$

where α is the spin component with respect to the quantization axis of the polarizer. Then through the device, each plane wave is distorted and the two Majorana zones ($D_{\alpha\beta}$ and $D'_{\beta\gamma}$ Wigner rotation matrices) entangle the evolu-

tion of the magnetic components. Then the outgoing γ-polarized wave is written

$$\psi_\gamma^{\text{out}}(\mathbf{r}, t) = \int \sum_\beta d^3k\, C_\alpha(\mathbf{k})\, D_{\alpha\beta}(\mathbf{r}, t)\psi_P(\mathbf{k}; \mathbf{r}, t)e^{i\varphi(\mathbf{k},\beta;\mathbf{r},t)/\hbar} a(\mathbf{k}; \mathbf{r}, t) D'_{\beta\gamma}(\mathbf{r}, t) \quad (2.10)$$

The plane wave expansion of this wave is

$$\psi_\gamma^{\text{out}}(\mathbf{r}, t) = \int d^3l\, D_\gamma(\mathbf{l})\psi_P(\mathbf{l}; \mathbf{r}, t) \quad (2.11)$$

Neglecting the $(\mathbf{r}, t)$ dependence in the Wigner rotation matrices, the comparison of (2.10) and (2.11) leads to

$$D_\gamma(\mathbf{l}) = \sum_\beta \int d^3\, k\, C_\alpha(k) D_{\alpha\beta} D'_{\beta\gamma} e^{-i\hbar[(k^2 - l^2)/2M]t} b(\mathbf{k}, \mathbf{l}; \beta, t) \quad (2.12)$$

where

$$b(\mathbf{k}, \mathbf{l}; \beta, t) = \int \frac{d^3r}{(2\pi)^3}\, a(\mathbf{k}; \mathbf{r}, t)e^{i[(\mathbf{k}-\mathbf{l})\mathbf{r}+\varphi(\mathbf{k},\beta;\mathbf{r},t)/\hbar]}$$

is the entanglement term, depending on the form of φ. It can be expressed as a series [e.g., a series of Bessel functions, for a potential sinusoidal in $\mathbf{r}$ and t; see Mathevet (1998)].

Assuming that the detector is sensitive to plane waves, the coherent part of the signal is

$$s = \int d^3l\, |D_\gamma(\mathbf{l})|^2$$

We introduce the statistical averaging effects by setting $C_\alpha(\mathbf{k}) \equiv C_\alpha(\mathbf{k}, \underline{a})$, $\underline{a}$ being a set of parameters distributed with the probability density $\rho(\underline{a})$. Then the final signal S is

$$S = \int d\underline{a}\, \rho(\underline{a})\, s(\underline{a})$$

The set of parameters $\underline{a}$ is related to the beam velocity distribution (or to a partial magnetic polarization). This will reduce the fringe contrast (obtained by the scan of one of the experimental parameters) in an *inhomogeneous* way. Other losses of contrast have a homogeneous origin (they are related to amplitudes, not to intensities). They define the "finesse" of the interferometer or the *homogeneous* width. The ingredients in $D_\gamma(\mathbf{l})$ are related to the perturbation of the wave induced by the interaction. This is a general feature of wave equations (Eckart, 1948): whatever the wave equation is, its amplitude perturbation follows a Schrödinger-like equation. To be able to test the wave

itself, we need to know how to measure the phase velocity. In its complex form, quantum mechanics does not show a way to succeed in this direction.

We have not used here a direct calculation using density operator techniques in spite of the fact that they are convenient to describe coherence properties. The reason is that in the continuum case it is much easier and more pedagogical to compute this operator from the wave function and then make a statistical averaging.

3. EXPERIMENTAL ILLUSTRATIONS

Our experiment uses a beam of metastable hydrogen atoms (spin 1) whose velocity distribution is peaked at 10 km/s. The experimental scheme has been described in detail elsewhere (Robert, 1992) and is shown in Fig. 3. Here we present results on the longitudinal Stern–Gerlach effect, revealed by time of flight, and we discuss the problem of coherence through the Humpty Dumpty effect (Schwinger, 1989).

3.1. Longitudinal Stern–Gerlach Effect

For a one-dimensional problem (static transverse magnetic field profile) and assuming a perfect magnetic state preparation and analysis, one gets

$$\varphi(k, \mathbf{r}, t) = \frac{1}{v}\int V_\beta(u)\, du = \frac{A\beta\hbar}{k} \tag{3.1}$$

$$b = e^{iA\beta/k}\int \frac{d^3r}{(2\pi)^3}\, a(\mathbf{r} - \frac{\hbar\mathbf{k}}{m}t)e^{i(\mathbf{k}-\mathbf{l})\mathbf{r}} \tag{3.2}$$

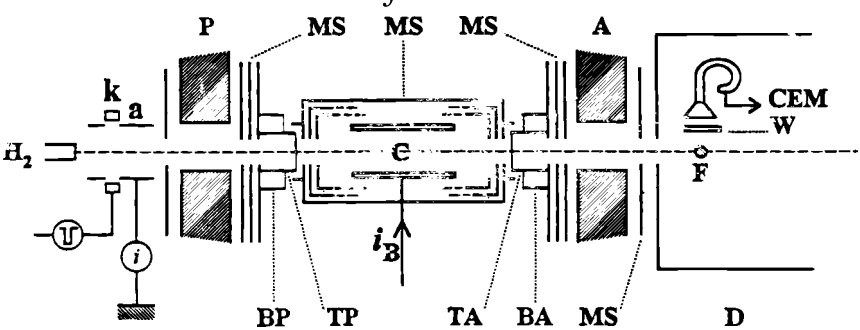

Fig. 3. Scheme of the apparatus. H_2+k+a, Metastable hydrogen source; P, A, polarizing and analyzing magnetic fields; BP + TP and BA + TA, slow and fast commutators of polarization guiding fields; C, phase device supplied by the current i_B; MS, magnetic screens and shields; F + W + CEM, metastable hydrogen detector (F is the quenching electric field, W is the MgF_2 window, and CEM is the channeltron electron multiplier).

The function a is unknown: it expresses the synchronization of the atomic wave function with the detector. For simplicity we choose it as defining one velocity (by time of flight). Then

$$b = e^{iA\beta/k}\delta(\mathbf{k} - \mathbf{l})\delta(\mathbf{k} - \mathbf{k}_0) \tag{3.3}$$

Using this expression in (2.12), one gets

$$D_\gamma(\mathbf{l}) = \sum_\beta C_\alpha(\mathbf{l}) D_{\alpha\beta} D'_{\beta\gamma}\, e^{iA\beta/l}\delta(\mathbf{l} - \mathbf{k}_0) \tag{3.4}$$

$$s = |C_\alpha(k_0)|^2 \left| \sum_\beta D_{\alpha\beta}\, D'_{\beta\gamma}\, e^{iA\beta/k_0} \right|^2 \tag{3.5}$$

Finally

$$S = \int d\underline{a}\, \rho(\underline{a}) |C_\alpha(\underline{a}, \mathbf{k}_0)|^2 \left| \sum_\beta D_{\alpha\beta} D'_{\beta\gamma}\, e^{iA\beta/k_0} \right|^2 \tag{3.6}$$

where $\rho(a)$ takes into account the velocity incertitude in the experimental realizatio
experime

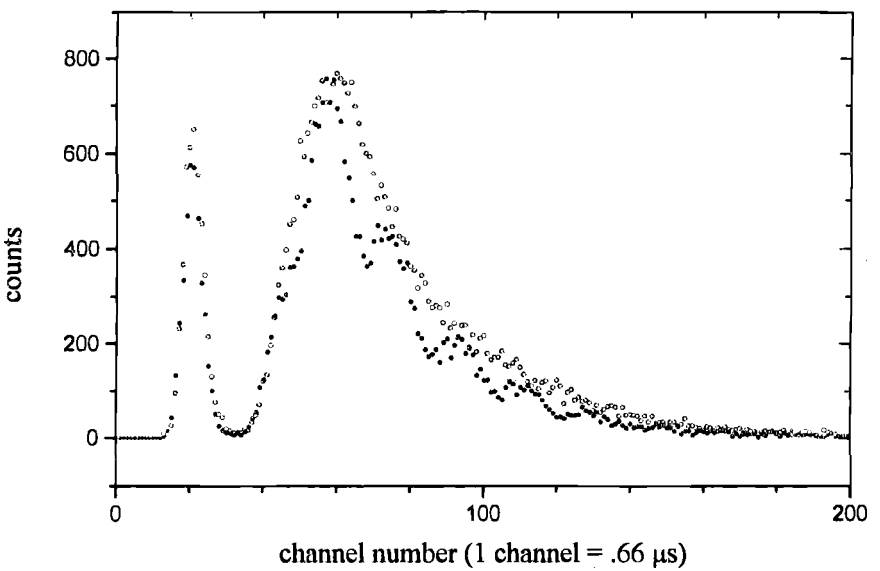

Fig. 4. Example of a time-of-flight experiment. Open circles: TOF with a phase shift equal to zero. Full circles: TOF with a phase shift of 2π for the most probable velocity corresponding to a current of 1 A in the phase device. Notice in the latter the linear time dependence of the oscillations.

$$S(\tau) = |C_\alpha(\tau)|^2 \left| \sum_\beta D_{\alpha\beta} D'_{\beta\gamma} e^{iA'\beta\tau} \right|^2 \tag{3.7}$$

which means that the argument of the oscillations seen in Fig. 4 is proportional to τ.

3.2. Loss of Coherence, Humpty Dumpty Effect

The preservation of spin coherence through a Stern–Gerlach interferometer was theoretically studied by Schwinger and co-workers (1988). The main idea is to cut the central region into two successive zones and try to balance the effect of the first zone by that of the second. We realized that scheme as described in Fig. 5 (Nic Chormaic *et al.*, 1994).

A detailed computation can be found in Lawson-Daku (1997) that fits fairly well with the experimental results. The analysis presented in Section 2 shows that there exists a coherent effect with respect to the transverse direction, resulting in a "coherent" loss of the fringe contrast. The rays have histories depending on the impact parameter. Actually both the Majorana transition coefficients and the dephasing terms depend on the impact parameter as soon as the magnetic field profile is transversely inhomogeneous. As a result, the coherence properties are very sensitive to transverse field gradients. Now, if one expresses the 1D signal as a function of the magnetic field magnitude, assuming that the detector is permanently open, one gets

$$b = e^{iA\beta/k} \delta(\mathbf{k} - \mathbf{l}) \tag{3.8}$$

and then

$$S(A) = \int d\underline{a}\, \rho(\underline{a}) \int d^3 l\, |C_{\underline{a}}(\underline{a}, \mathbf{l})|^2 \left| \sum_\beta D_{\alpha\beta} D'_{\beta\gamma} e^{iA\beta/l} \right|^2$$

Here $|C_{\underline{a}}(\underline{a}, \mathbf{l})|^2$ is due to the averaging over the transverse section of the interferometer and corresponds to the width for the 1D expression of the signal. We have shown that it is possible to separate the longitudinal $\rho(\underline{a})$ contribution from the transverse one $|C_{\underline{a}}(\underline{a}, \mathbf{l})|^2$ by improving the velocity selection. Figure 6 shows that the interferometer fringe resolution has an intrinsic limitation. This limitation is due to the inhomogeneity of the magnetic field profile. With an improved field configuration we have shown (Fig. 7) that it is possible to shift the central fringe obtained with the broad velocity distribution over a range of magnetic field broader than that defined by the inhomogeneous width.

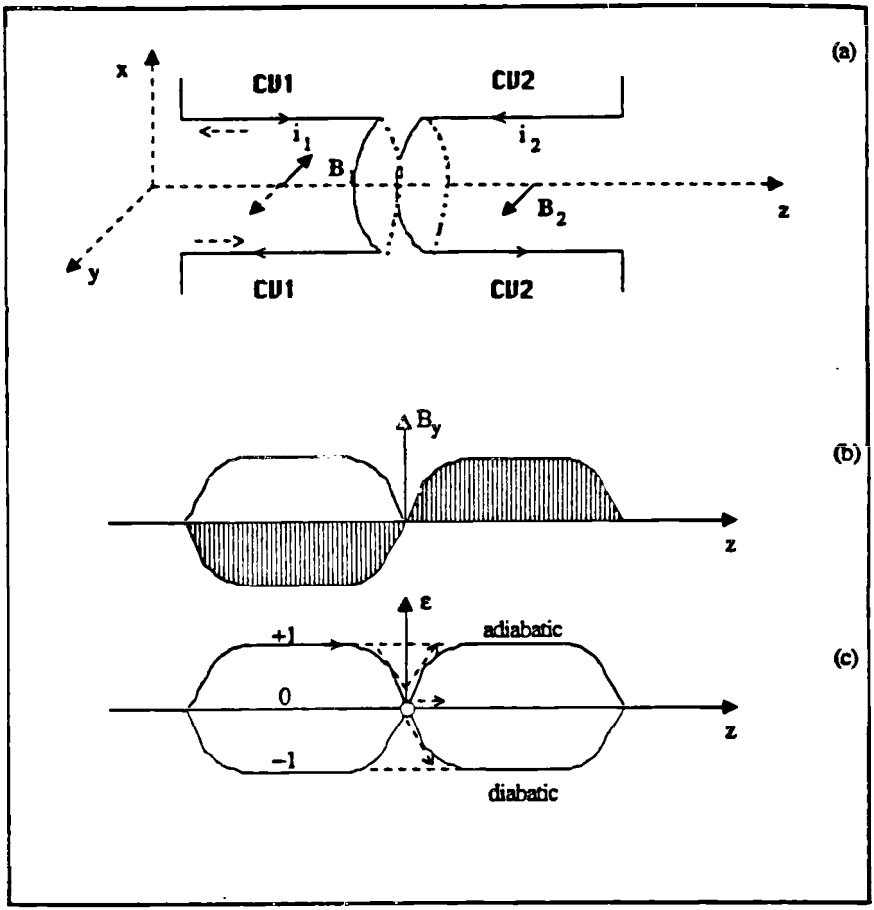

Fig. 5. (a) Schematic representation of the two frames, CV1 and CV2, showing the directions of current flow which were considered and the resulting transverse magnetic field in the $+y$ or $-y$ direction. (b) The shaded area represents the gradients when i_1 and i_2 are flowing in opposite directions. (c) A schematic representation of the different spin evolutions which are equivalent to adiabatic and diabatic transitions. In each of these diagrams z is the direction of propagation of the atoms.

This effect reveals that the loss of coherence in an interferometer is strongly dependent on the number of variables that are entangled because each of them affect the phase definition. To get "perfect" fringes one must be able to achieve a clean separation between the variables involved in the phase and the other ones. This would allow one to realize interferences independently of the object size.

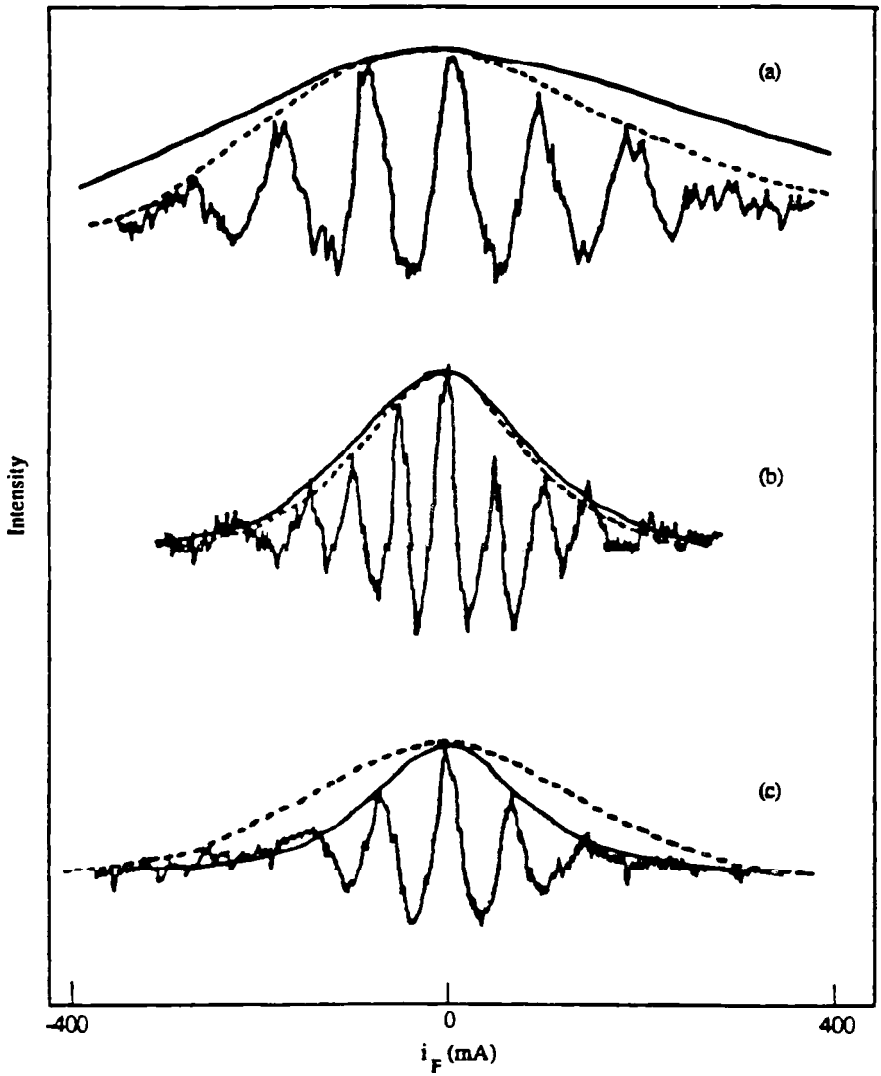

Fig. 6. Interference patterns obtained using the single-frame interferometer for three different velocity selections: (a) $\delta v/v = 13\%$, $v_{av} = 9.4$ km/s, (b) $\delta v/v = 20\%$, $v_{av} = 4.5$ km/s, (c) $\delta v/v = 40\%$, $v_{av} = 6.9$ km/s. The current in the frame is scanned from -400 to $+400$ mA. Full line: envelope for the velocity distribution assuming a constant phase shift.

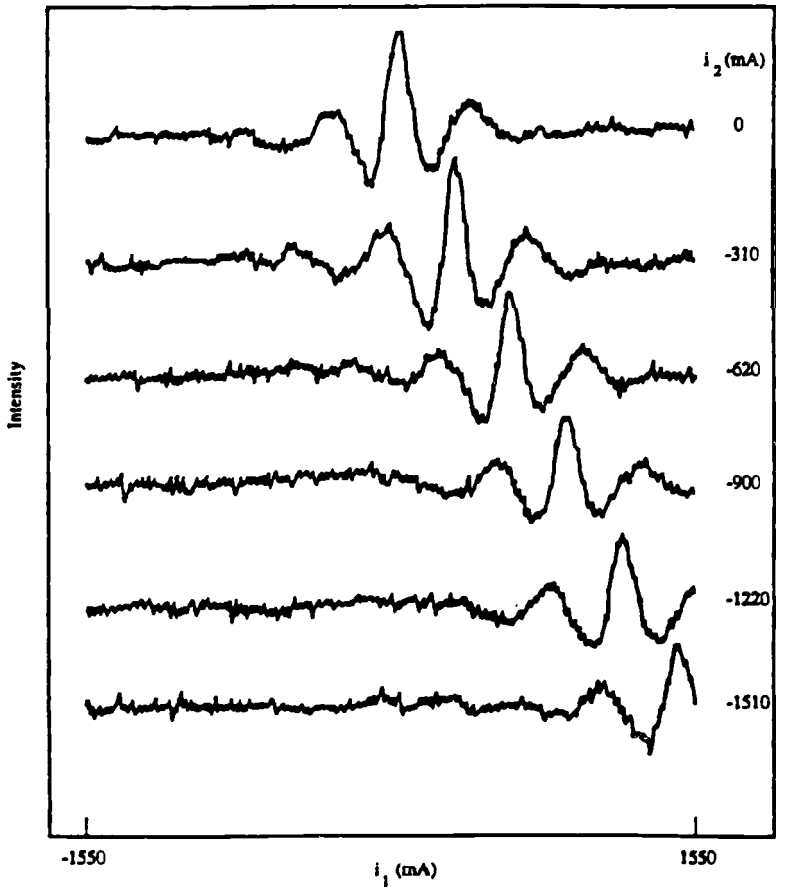

Fig. 7. Interference pattern obtained for the improved double-frame configuration by scanning i_1 from -1550 to $+1550$ mA while keeping i_2 fixed.

4. OPTICAL EFFECTS. BEADED ATOMS

4.1. Beaded Atoms

If one looks at formula (2.10) in terms of virtual interfering sources, one has to express the outgoing wave function in terms of a summation over displacement operators acting on the incident wave function. However, in order to achieve this and because of the wavenumber dispersion (except for topological or geometrical nondispersive phases) (Nic Chormaic, 1994) one has to treat the problem using wave packets rather than infinite plane waves. As a matter of fact, in order to act on a wave, we have to perturb it. Therefore, even at the lowest order of perturbation, this leads us to consider a wave

packet within a restricted interval in space and time. For instance, in the case of a scattering problem, even the so-called incident plane wave has to be a wave packet having a restricted extension in space. That is why wave packets are implicit in most of that kind of work (Joachain, 1979).

This point has, of course, to be used in harmony with the strong rule that transition probabilities are defined with respect to wave-packet expansion components, as shown by the transition of unresolved waves to resolved waves (Eckart, 1948). The remaining question is how to determine what kind of properties can be stored into a wave in order to attribute them to a corresponding atom, provided that this has any significance in a wave picture.

The general Fourier expansion of the solution of our problem (2.10) and (2.11) shows through (2.12) that in the case where

$$b(\mathbf{k}, \mathbf{l}, \beta, t) = \delta(\mathbf{k} - \mathbf{l}) e^{i\theta(\mathbf{k},\beta)} \tag{4.1}$$

the $D(\mathbf{l})$ factor is for each β in a 1–1 correspondence with $C(\mathbf{k})$. This means that there is no net force acting on each spin term and that the output term is on the same momentum-energy shell as the incoming one (longitudinal SG effect). Under these restricted circumstances the arguments of the wave Fourier components can be written

$$\mathbf{k} \cdot \mathbf{r} - \frac{\hbar k^2}{2M} t + \theta(\mathbf{k}, \beta) = \mathbf{k} \cdot (\mathbf{r} - \delta_\beta \mathbf{r}) - \frac{\hbar k^2}{2M} (t - \delta_\beta t) \tag{4.2}$$

where $\delta_\beta \mathbf{r}$ and $\delta_\beta t$ are constructed in order to satisfy the equality. There are two limiting choices: (i) when all the dephasing effect is on $\mathbf{r}$: $(\Delta_\beta \mathbf{r})$; (ii) when the whole effect is reported on t: $(\Delta_\beta t)$.

We assume that the quasi-plane-wave approximation is not too bad to represent what has to be called "an atom." The "passing through" the interferometer transforms each atom amplitude into a sum of atom amplitudes phase shifted by a factor $\exp(i\mathbf{k}\cdot\Delta_\beta \mathbf{r})$. This $\Delta_\beta \mathbf{r}$ factor can thus be viewed as a wave modulation term or as a wave packets center splitting term, giving rise to a beaded atom by analogy with a necklace (Miniatura, 1991). In our opinion, this phraseology is relevant only if it can lead to "new" properties for the atoms. The magnitude of the chosen magnetic field intensity determines $\Delta_\beta \mathbf{r}$ in the interferometer, and an easy numerical calculation shows that for hydrogen metastable atoms experiencing a homogeneous magnetic field B acting over a length L, $|\Delta_\beta \mathbf{r}| = \Delta_\beta z$ is given by

$$k\Delta_\beta z = \beta \frac{g\mu_B BL}{v} = F\tau \tag{4.3}$$

or

$$\Delta_{\beta z} = \beta \frac{g\mu_B BL}{\hbar k v} = \beta \frac{g\mu_B BL}{Mv^2} = G\tau^2 \tag{4.4}$$

where τ is the time of flight over the length L, and F and G are constants. Therefore, the beaded atom properties will be clearly separated from the other wave-modulation properties only in a time-of-flight measurement exhibiting periodic oscillation as a function of τ^2.

4.2. Spontaneous Emission of Beaded Atoms

In a naive way, such a beaded atom could be seen in a classical analogy as an array of (correlated) antennas which should exhibit remarkable electromagnetic properties. We have tested the effect of a splitting of the order of the optical wavelength. This corresponds to a B field magnitude of the order of 1000 G. In Fig. 8 we present a set of experimental results. One can see oscillations whose periodicity is quite different from that of Fig. 4. Another feature is the signal dependence on the observation direction, which seems to reflect classical properties of the radiation emitted by the antenna array.

From this point of view, all these results seem very clear. However, they raise the important question of the correct interpretation. Indeed, up to now, spontaneous emission calculations of moving atoms have not been able to reproduce the results. The main reason is the inclusion of recoil terms in the theory of spontaneous emission, which completely destroys the correlation among the emitters. As a result all "wave packet effects" disappear (Cohen, 1992, Steuernagel, 1996). An analysis of these wave packet effects in atom–light interaction is in progress (Stoop, 1997; Pumares, 1997). Nevertheless, the theory is not yet able to account for the experimental modulations that we have observed. One point is to be noticed: none of these calculations has used the improved form computed in the canonical approach that includes the so-called Röntgen terms (Baxter, 1993; Lembessis, 1993). Their structure entangles dipole terms with center-of-mass and electromagnetic terms; nevertheless, it is hard to say if such terms are able to give a correct result without any further detailed calculations.

5. CONCLUSION

Atom interferometry is situated on the coherent side of the decoherence problems. We have learned that under our experimental conditions, which are not too restrictive, the interference ability of a quantum system is strongly related to the degree of entanglement among its master variables. When all of them are fairly controlled, we can obtain patterns with high contrast as

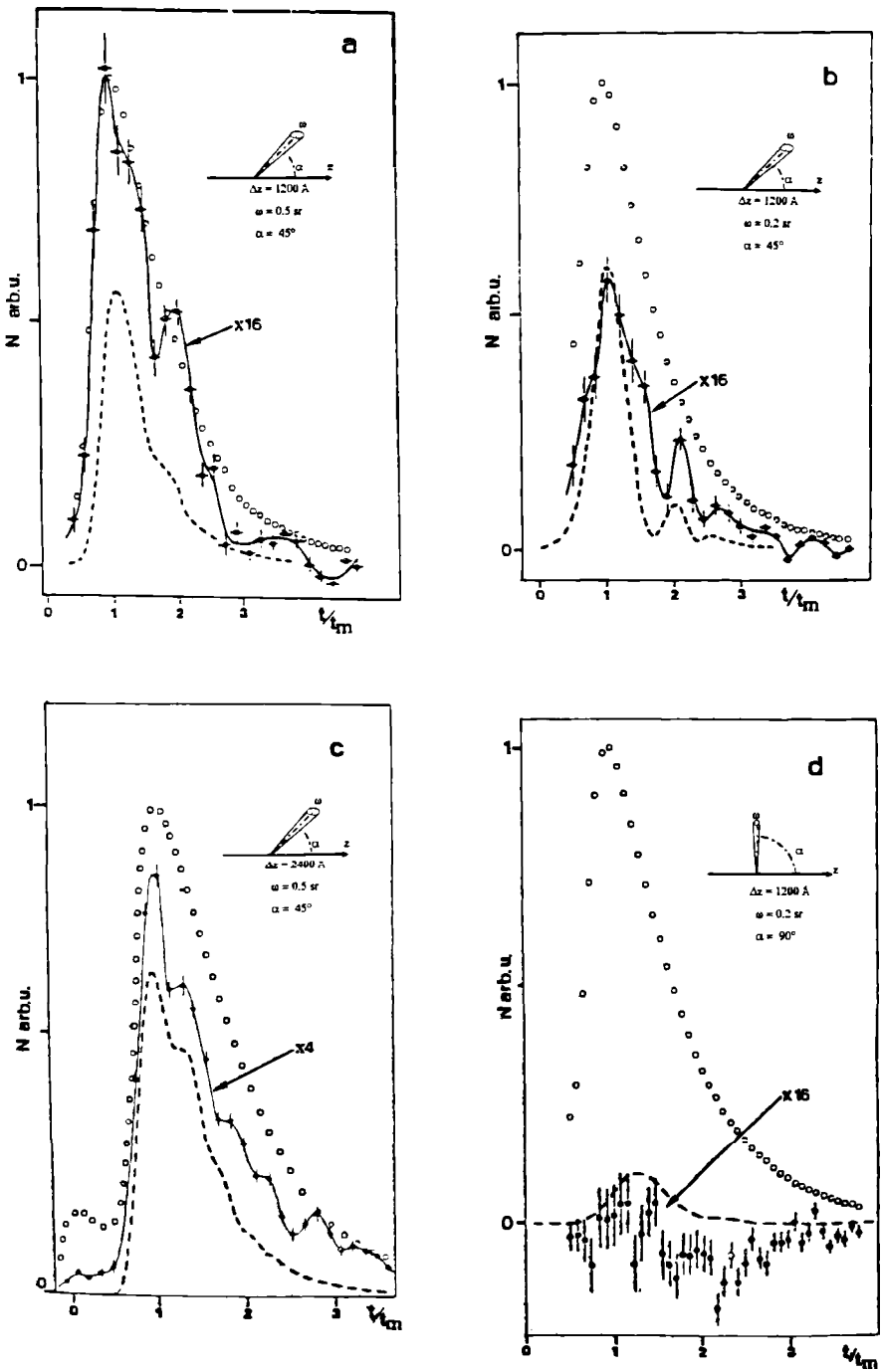

Fig. 8. Time-of-flight spectra in the presence of a strong longitudinal magnetic field $B_{\|}$. Open circles: TOF spectra with $B_{\|} = 0$ normalized such that the maximum value is 1. Full circles and full lines: difference Δ between spectra without and with $B_{\|}$. Broken curve: calculation of Young's holes. Panels (a), (b), and (d) were obtained with $\int B_{\|}\, dz = 1000\text{G}\cdot\text{cm}$, panel (c) with $\int B_{\|}\, dz = 2000\ \text{G}\cdot\text{cm}$.

shown in Fig. 4. If not, the wavefront distortions, combined with classical statistical averaging effects, induce decoherence due to the inhomogeneities in the entanglement. To do science fiction, one could even imagine making interferences with macroscopic objects. It only requires really separating a set of variables from all the others, namely isolating the phase carrier variables from all the other variables. The relevance of the concept of "beaded atoms" remains an open question. All this reveals at the same time the difficulty, but also the versatility of tailoring quantum phases by atom interferometry.

ACKNOWLEDGMENTS

J.B.L.D.'s work was support by a Nicolas-Claude Fabri de Peiresc grant via the Association Louis de Broglie d'Aide à la Recherche. J.R. wishes to acknowledge D. Aerst, S. Diner, T, Durt, and E. Gunzig for the kind invitation to present this work in Peresq. We also acknowledge the great and warm hospitality of Mady Smets and her team.

REFERENCES

Baudon, J. *et al.* (1998). *Comments in Atomic and Molecular Physics*, to appear.
Baxter, C., *et al.* (1993). *Phys. Rev. A* **47**, 1278.
Bloom, M., and Erdman, K. (1962). *Can. J. Phys.* **40**, 179.
Cohen Tannoudji, C., *et al.* (1992). In *Proceedings of the 10th International Conference on Laser Spectroscopy*, M. Ducloy *et al.* eds., Word Scientific, Singapore.
DeKieviet, M., *et al.* (1995). *Phys. Rev. Lett.* **75**, 1919.
Eckart, C. (1948). *Rev. Mod. Phys.* **20**, 399.
Frisch, O. R., Von Halban, H., Jr., and Koch, J. (1938). *Phys. Rev.* **53**, 719.
Glauber, R. J. (1959). In *Lectures in Theoretical Physics*, Vol. 1, W. E. Brittin and L. Dunham, eds., Interscience, New York.
Joachain, Ch. J. (1979). In *Quantum Collision Theory*, North-Holland, Amsterdam, Vol. 1, p. 55.
Lawson Daku, J. B. (1997). Thèse de Doctorat, Université Paris Nord, France.
Lawson Daku, J. B., *et al.* (1996). *Phys. Rev. A* **54**, 5042.
Lembessis, V. E., *et al* .(1993). *Phys. Rev. A* **48**, 1594.
Mathevet, R. (1998). Thèse de Doctorate, Université Paris Nord, France.
Mathevet, R., *et al.* (1997). *Phys. Rev. A* **56**, 2954.
Mezei, (1986). *Physica* **137B**, 295.
Miniatura, C., *et al.* (1991). *J. Phys. II France* **1,** 425.
Nic Chromaic, S. (1994). Thèse de Doctorat, Université Paris Nord, France.
Nic Chromaic, S., *et al.* (1994). *Phys. Rev. ett.* **72**, 1.
Pumares L., *et al.* (1997). *Phys. Rev. A* **55**, 4386.
Rabi, I. (1937). *Phys. Rev.* **51**, 652.
Robert, J., *et al* (1991). *Europhys. Lett.* **16**, 29.
Robert, J., *et al.* (1992). *J. Phys. II France* **2**, 601.
Schwinger, J. (1937). *Phys. Rev.* **51**, 648.

Schwinger, J., *et al*. (1988). *Z. Phys. D* **10**, 135.
Sokolov, Y. L. (1973). *Sov. Phys. JETP* **36**, 243.
Sokolov, Y. L. (1996). *Physica Scripta* **54**, 156.
Steuernagel, O., and Paul, H. (1996). *Phys. Rev. A* **53**, 2983.
Stoop, H., *et al*. (1997). *Phys. Rev. A* **55**, 2254.